RSC Advances

PAPER

View Article Online
View Journal | View Issue

Cite this: *RSC Adv.*, 2024, **14**, 32602

Composite microarc oxidation coatings containing Cu on titanium alloy

Zaiqiang Feng,[a] Chenxi Li,[a] Chang Xin,[a] Zhengquan Jiang,[a] Zhenwei Yan,[b] Wen Wang,[b] Ningning Li,[a] Zhaojun Tan[b] and Mingqi Tang *[a]

A soft and hard composite MAO coating was prepared by adding Cu particles to an alkaline phosphate-borate electrolyte to modify the MAO coating on titanium alloy. The effects of Cu particles on the thickness, structural features, and friction characteristics of the MAO coating were investigated. The MAO coating formed in Cu particle-free electrolyte mainly comprised rutile and anatase TiO_2. Cu and CuO were detected in the oxide coatings obtained in the electrolyte with Cu particles. The hardness of the coating prepared in the base electrolyte was approximately 420 HV, whereas that obtained in the electrolyte containing 2 g L^{-1} Cu particles increased to 470 HV. While the friction coefficient of the base MAO coating exhibited significant fluctuations, the friction coefficient of the MAO coating containing Cu particles remained relatively stable. The MAO coating formed in the electrolyte containing 2 g L^{-1} Cu particles demonstrated superior frictional performance, exhibiting a value approximately 3.6 times higher than the base coating. Cu particles enter the MAO coating through electrophoresis, mechanical agitation, and micro-melt adsorption to improve the compactness of the coating. Due to the excellent plasticity of Cu, the friction properties of Cu-containing MAO coating were enhanced.

Received 27th August 2024
Accepted 6th October 2024

DOI: 10.1039/d4ra06194b

rsc.li/rsc-advances

1. Introduction

Titanium alloys have excellent mechanical, physical, and chemical properties and are widely used in various sectors such as aerospace, petrochemicals, shipbuilding, and medical equipment.[1,2] However, titanium alloys have the problems of low hardness and poor abrasion resistance, which limit their application areas to some extent. Compared with traditional anodic oxidation, the forming conditions of high-pressure discharge of the MAO can form ceramic-like oxide coatings with high hardness, corrosion resistance, tribological properties, and metallurgical bonding with titanium alloy.[3–5]

The MAO coatings on titanium alloy mainly comprise TiO_2 and components derived from the electrolyte. Although its hardness is significantly enhanced compared with titanium alloy, it suffers from the problems of poor toughness and brittleness. In addition, the MAO coating formation process is accompanied by intense spark discharge and gas escape, and some holes, cracks, and other defects will inevitably appear in the MAO coating with insufficient densification.[6,7] To reduce the defects and improve the performance of the MAO coating, researchers have added micro- or nano-particles to the electrolyte. These particles enter the oxide coating under the combined action of electrophoresis, mechanical stirring, and micro-discharge reaction, reducing the defects in the MAO coating, thus obtaining a density and antifriction coating.[8–11]

Therefore, some hard particles with excellent mechanical and thermomechanical properties, such as Al_2O_3, Cr_2O_3, ZrO_2, NbC, WC, SiC, *etc.*, have been used to improve MAO coatings' microstructure and tribological properties.[12–15] Li *et al.* investigated the influences of α-Al_2O_3, Cr_2O_3, and h-BN particles on the structural features and properties of the MAO coatings.[14] The microstructures of the MAO coating were improved using well-dispersed WC particles as electrolyte additives. Compared to the ordinary MAO coating, the wear resistance and corrosion resistance of SiC composite MAO coating were better.[15]

Hard particles can significantly enhance the hardness and tribological properties of the MAO coatings. However, during the friction process, flaking MAO coating fragments cause abrasive wear and exacerbate the damage to this brittle oxide coating. Therefore, the researchers explored using self-lubricating particles as electrolyte additives to obtain composite MAO coatings with self-lubricating properties.[16–18] Mu *et al.*[16] prepared a fine and smooth self-lubricating MAO coating in an electrolyte with graphite particles. They thought that the worn MAO coating surface underwent a process of "formation–destruction–repair–formation." During this process, graphite particles mixed with abrasive debris were transferred to form a "lubrication film" on the steel ball. In addition, Mu *et al.*[17] revealed the mechanism of MoS_2 in reducing the MAO coating's friction coefficient and wear rate.

[a]*School of Materials Science and Engineering, North China University of Water Resources and Electric Power, Zhengzhou 450045, China. E-mail: tangmq400@163.com*

[b]*School of Mechanical Engineering, North China University of Water Resources and Electric Power, Zhengzhou 450045, China*

MoS_2 particles migrated to the opposing friction pair surface during the sliding test and lubricated, enhancing the MAO coatings' tribological properties.

Cu and some Cu alloys have good plasticity, which can significantly reduce the friction coefficient between friction pairs, and are often used as wear-resistant anti-friction materials.[19,20] The main methods for obtaining Cu alloy anti-friction layers on titanium alloys are cladding, electroplating, plasma spraying, double glow plasma surface alloying.[21–24] However, these methods have their limitations. For example, the surface accuracy of the cladding layer is poor, and the adhesion between the plasma spraying and electroplating Cu layer and the titanium alloy matrix is poor. Therefore, by introducing Cu particles into the MAO electrolyte for titanium alloy, the Cu particles can reduce the cracks, micropores, and other defects in the MAO coating. Furthermore, Cu particles are widely used as friction-reducing additives due to their particular surface area, easy plastic deformation, and low shear strength.[25] Therefore, the Cu particles incorporated in the MAO coatings can act as friction-reducing agents, thus improving the tribological properties of the MAO coatings.

In this work, composite MAO coatings were fabricated in the electrolyte containing different contents of Cu particles. The influences of Cu particles on the structural features and tribological properties of the composite oxide coatings were investigated.

2. Material and methods

The Ti_6Al_4V alloy blocks (20 mm × 20 mm × 4 mm) were polished with 180#–800# SiC grit paper to remove the oxidized layer, cleaned with acetone and DI water, dried with hot air, and then treated with MAO. The equipment used in the MAO process includes a pulsed power supply (JX-MAO, Lanzhou Jingxin Power Supply Co., Ltd.), an electrolyte chamber, an electric stirrer, and a circulating water-cooling system. The MAO power supply was used in constant current mode. The current density, frequency, duty cycle, and oxidation time were set to 8 A dm^{-2}, 300 Hz, 25%, and 40 min, respectively. A stainless steel plate was used as the cathode, and a Ti_6Al_4V alloy sample was used as the anode. The base electrolyte composition and electrical parameters were described in ref. 13. The base electrolyte was $(NaPO_3)_6$ (10 g L^{-1}), $Na_2B_4O_7 \cdot 10H_2O$ (8 g L^{-1}), NaOH (4 g L^{-1}), and $Na_2SiO_3 \cdot 9H_2O$ (2 g L^{-1}). Additionally, an additive of 1–3 g L^{-1} of 200 nm Cu particles (Hebei Leber Metal Material Technology Co., Ltd.) was incorporated to produce composite MAO coatings containing Cu. After ultrasonic dispersion for 1 h, the pH, conductivity, and zeta potential of the electrolyte were measured using a pH meter (PHS-3E), a conductivity meter (DDSJ-308F), and a zeta potential meter (Zetasizer Nano ZS90) at 25 °C, respectively. Table 1 lists the electrolytes' pH, conductivity, and zeta potential. The electrolyte with Cu particles was pre-stirred for 1 hour before the MAO treatment and continuously stirred during the MAO process.

Scanning electron microscopy (SEM, TESCAN VEGA) equipped with energy spectrometry (EDS, Bruker QUANTAX) was used to study the coatings' surface, cross-sectional morphology, and element compositions. X-ray diffraction (XRD, Rigaku Smart Lab) was used to scan the samples in the 10°–80° range at a rate of 6° min^{-1} and in combination with X-ray photoelectron spectroscopy (XPS, Thermo Fisher Nexsa) to determine the phase and elemental composition of the MAO coatings (Table 2). XPS was performed using Al Kα (photon energy 1486.6 eV) as the X-ray source and C 1s the reference. According to the research results of Hultman's team, the peak value of C 1s was closely related to the work function (Φ_{SA}) of the sample, and cannot simply be used as a reliable reference for calibration of the binding energy (E_B).[26–32] Therefore, the binding energy of C 1s was calibrated using the formula $E_B + \Phi_{SA} = 289.58$ eV,[28] where the TiO_2 work function Φ_{SA} was 5.20 eV,[33] then the E_B of the C 1s peak was 284.38 eV. XPS spectra were fitted by the "XPSPEAK" software using a Shirley background and Gaussian–Lorentzian peak shapes.

Table 1 Values of pH, conductivity, and zeta potential of different electrolytes at 25 °C

Electrolyte	pH	Conductivity (mS cm^{-1})	Zeta potential (mv)
0 g L^{-1} Cu	12.58	14.50	−14.6
1 g L^{-1} Cu	11.97	15.33	−13.2
2 g L^{-1} Cu	11.69	15.67	−12.1
3 g L^{-1} Cu	11.56	15.81	−11.3

Table 2 Elemental content of the MAO coating obtained in different electrolytes

Electrolyte	O (at%)	Al (at%)	P (at%)	Ti (at%)	Si (at%)	Cu (at%)
0 g L^{-1} Cu	70.79	1.53	8.13	17.84	1.70	—
1 g L^{-1} Cu	67.66	1.99	10.83	16.47	1.86	1.19
2 g L^{-1} Cu	67.15	2.02	8.82	17.17	1.79	3.05

The hardness and friction properties of the MAO coating were also tested as described in ref. 13. The MAO coatings' hardness was determined using a microhardness tester (MVD-1000JMT2) under 1 N load for 10 s. The hardness test was conducted on a polished cross-section sample, and the hardness of five structurally homogeneous and dense areas was tested and averaged. The friction properties of the MAO coatings were evaluated using a multifunction tribometer (Rtec, MFT-5000) under reciprocating sliding mode at room temperature. A friction substrate made of SUS440C stainless steel with a diameter of 4 mm was utilized. The test parameters included a load of 1 N, an amplitude of 10 mm, a frequency of 5 Hz, and a duration of 1200 s. After the friction tests, a 3D confocal microscope equipped with the Rtec was used to analyze the wear marks' morphology and measure the wear volume.

3. Results and discussion

3.1. Voltage–time behaviors

The variation of voltage with time in the MAO process at constant current can reflect the growth of the MAO coating. The voltage–

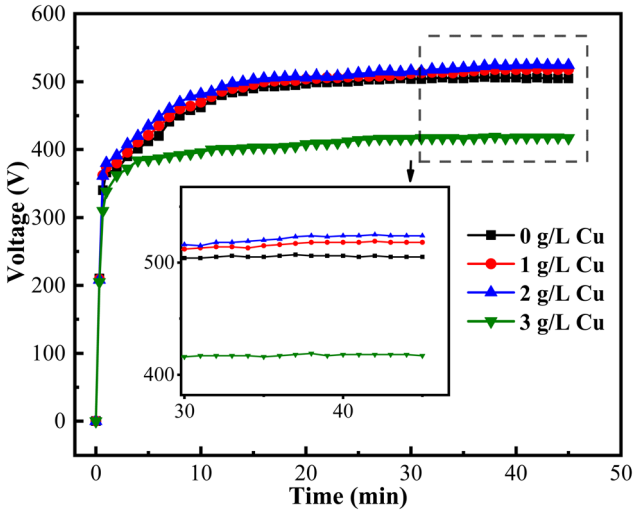

Fig. 1 Voltage variation with time in the electrolyte with different concentrations of Cu nanoparticles.

time curves for different contents of Cu particles in the electrolyte are displayed in Fig. 1. The voltage changes in the electrolytes with 0 g L^{-1}, 1 g L^{-1}, and 2 g L^{-1} Cu particles are similar, with a rapid voltage increase from 0 to 15 min, which slows down with time, and the final voltage stabilizes around 505 V, 518 V, and 524 V, respectively. The difference in the voltage–time curves is caused by the conductivity of the Cu particles and their participation in the MAO coating formation. As shown in Table 1, adding Cu particles increases the conductivity of the electrolyte. In general, an increase in the conductivity of the electrolyte decreases the final voltage. According to previous studies, particles in the electrolyte are involved in the formation process of the MAO coating, changing its composition and phase composition, which also causes a change in voltage. As a result, the time–voltage curves of the MAO process in electrolytes with varying levels of Cu particles show variations. However, when the Cu particle content in the electrolyte is 3 g L^{-1}, the voltage remains stable mainly after rising to about 417 V, and some dark brown spots appear on the MAO coating surface. This suggests that excessive addition of particles is detrimental to the MAO discharge reaction, which is consistent with other investigations.

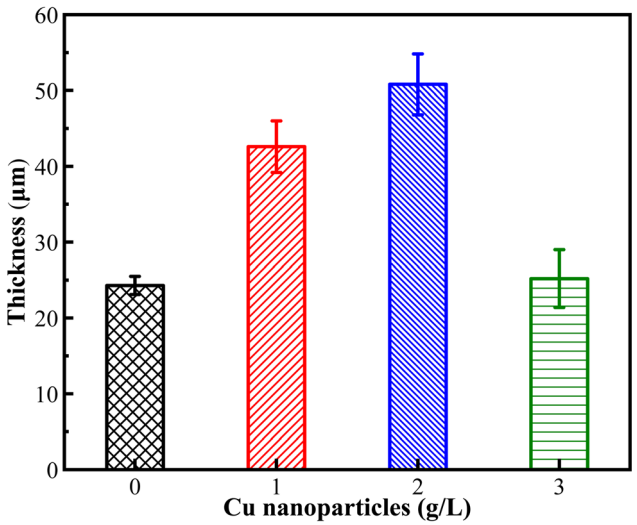

Fig. 2 Average thickness of the MAO coating in the electrolyte with different concentrations of Cu nanoparticles.

3.2. Coating thickness

Fig. 2 shows the MAO coating thickness obtained in electrolytes with different Cu particle contents. The average thickness of the coating formed in the base electrolyte is approximately 24.3 μm, and the average thickness of the oxide coatings produced in electrolytes containing 1–3 g L^{-1} Cu particles is 42.6 μm, 50.8 μm, and 25.2 μm, respectively. Compared to the base MAO coating, the thickness of the coatings prepared by adding 1 and 2 g L^{-1} Cu particles is increased by approximately 75% and 109%, respectively. This indicated that Cu particles participated in MAO coating formation and increased the coating formation rate. It was beneficial in reducing the energy consumption of the MAO technology. When the content of Cu particles is 3 g L^{-1}, not only does the thickness of the coating decrease significantly, but the surface of the coating also has many bumps with different colors and electrical erosion edges. The concentration of Cu particles in a specific range helps to improve the forming rate of MAO coatings, but too high is not conducive to growing the coating. Therefore, the MAO coatings fabricated in the electrolyte with 0–2 g L^{-1} Cu particles were investigated.

3.3. Morphologies features

Fig. 3 displays the macroscopic images and microscopic structures of the MAO coating produced in electrolytes containing varying concentrations of Cu particles. The coating prepared in the base electrolyte is light grey. After adding the Cu particles, the surface color of the coatings turns into a dark grey color, indicating that the Cu particles penetrate the MAO coating. Furthermore, the color of the base MAO coating is not homogenous. Adding Cu particles makes the color of the coating more uniform. The microscopic morphology of the three coatings shows some crater-like micropores and cracks on the surface, which is typical of MAO coating morphology. Influenced by the discharge plasma reaction and gas escape during the coating formation process of the MAO, these defects are of different sizes and depths due to the different intensities of the local plasma discharge reaction. As illustrated in Fig. 3(b), the pores on the coating surface decrease compared to the base coating after adding Cu particles, and the compact zone increases in the red-circled area.

When the Cu particles' content is 2 g L^{-1}, the compact region increases, and the number of pores significantly decreases, as shown in Fig. 3(c). In addition, Image J software was used to determine the surface porosity and pore size of the MAO coatings, and each data was measured three times and averaged to minimize errors. The results showed that the porosity of the base MAO coating is approximately 11%, and the maximum pore is about 20 μm. When the content of Cu particles in the electrolyte is 1 g L^{-1}, the porosity of the coating decreases to approximately 7%, and the maximum pore is about 16 μm. For

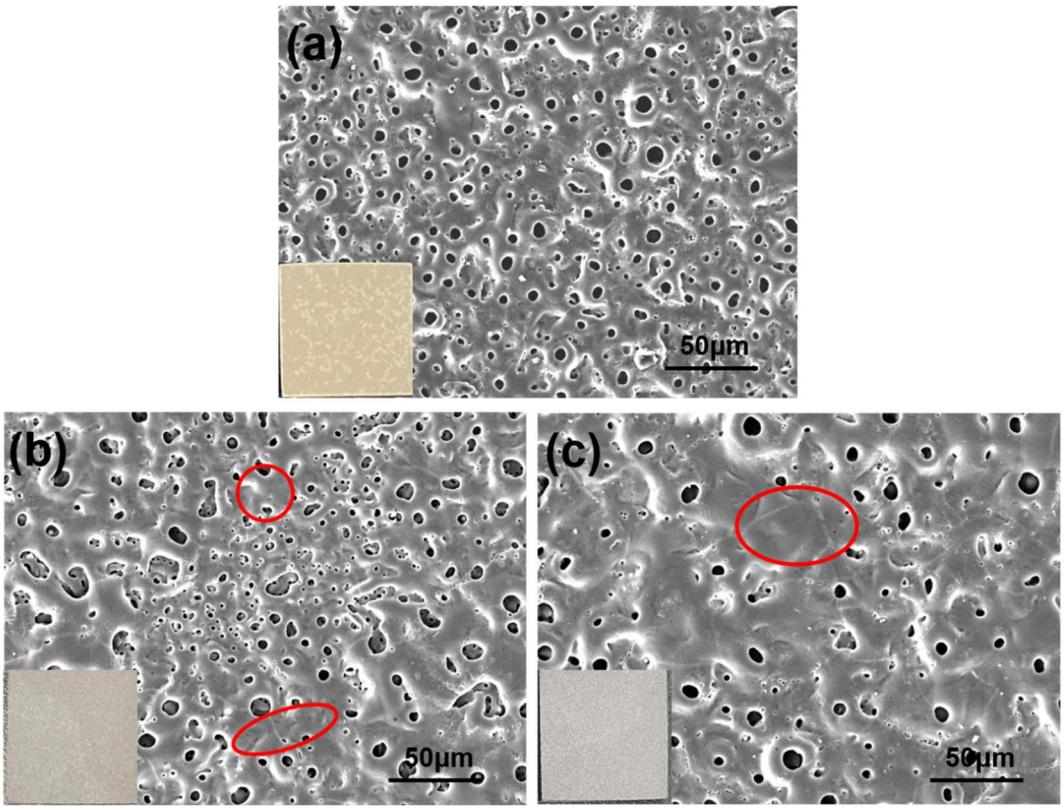

Fig. 3 Surface image of the MAO coating obtained in different electrolytes, (a) base electrolyte, (b) with 1 g L^{-1} Cu nanoparticles, (c) with 2 g L^{-1} Cu nanoparticles.

the MAO coating obtained in the electrolyte with 2 g L^{-1} Cu particles, its porosity decreases to approximately 5%, and the maximum pore is about 12 μm. Many studies have shown that adding micro and nanoparticles in the electrolyte can significantly improve the density of the MAO coating.[7,10] The particles can be doped into the surface layer or even inside the MAO coating during the oxidation process to repair the defect location of the coating and reduce defects such as holes and cracks.

Fig. 4 presents the cross-sectional morphologies of the MAO coating obtained in different electrolytes. The MAO coatings formed in the base electrolyte comprise a thin outer layer and a relatively dense inner barrier layer. The interior of the base MAO coating has many cracks and pores, and its densification is poor, as shown in Fig. 4(a). In contrast, the inner layer is relatively loose and porous for the coatings obtained in the electrolytes containing Cu particles, while the outer layer of the coating is denser. Moreover, three MAO coatings exhibit significant differences in thickness, and Cu particles significantly improve the coating thickness. Although a few noticeable pores still exist in the MAO coating prepared in the electrolyte with 1 g L^{-1} Cu particles, the densification increases considerably compared with the base coating. As the Cu particle content continues to grow, the overall structure of the oxide coating becomes more uniform and denser. Fig. 4 and Table 1 present the distribution and composition of the elements in the MAO coatings. The main components of the base coatings are O, Al, Si, P, and Ti, where Al and Ti come from the Ti alloy substrate, and O, P, and Si come from the electrolyte. Small amounts of Cu element could be identified in the MAO coatings obtained in electrolytes containing Cu particles. However, Cu is not uniformly distributed in the oxide coating, primarily in the outer part of the coating, as illustrated by the white arrows in Fig. 4(c). After forming the internal barrier layer of the oxide coating, the oxide process enters the microarc discharge stage, which is the rapid growth stage of the MAO coating.[7] Currently, many fast-moving white sparks occur on the anode surface. The electrical breakdown effect of spark discharge creates discharge channels in the MAO coating. Due to the small size and short duration of the sparks at the beginning of the microarc discharge, a small number of Cu particles enter the discharge channel by electromigration.[13] The Cu particles enter the MAO coating mainly by adhering to the melt produced by the sparks. With the increase of Cu particles in the electrolyte, the probability of adhesion to the spark discharge melt increases. Therefore, the Cu content is higher outside the MAO coating, as shown in Fig. 4(c).

The MAO coating fabricated in the electrolyte containing 2 g L^{-1} Cu particles was analyzed by XPS to determine the present form of the Cu element. Fig. 5(a) illustrates the full XPS spectrum of the MAO coating, which indicates that the oxide coating contains elements such as Na, O, P, Ti, and Cu. The appearance of the characteristic peak of Cu further shows that the Cu particles participate in the MAO coating. Fig. 5(b) displays the high-resolution XPS spectrum of Cu 2p,

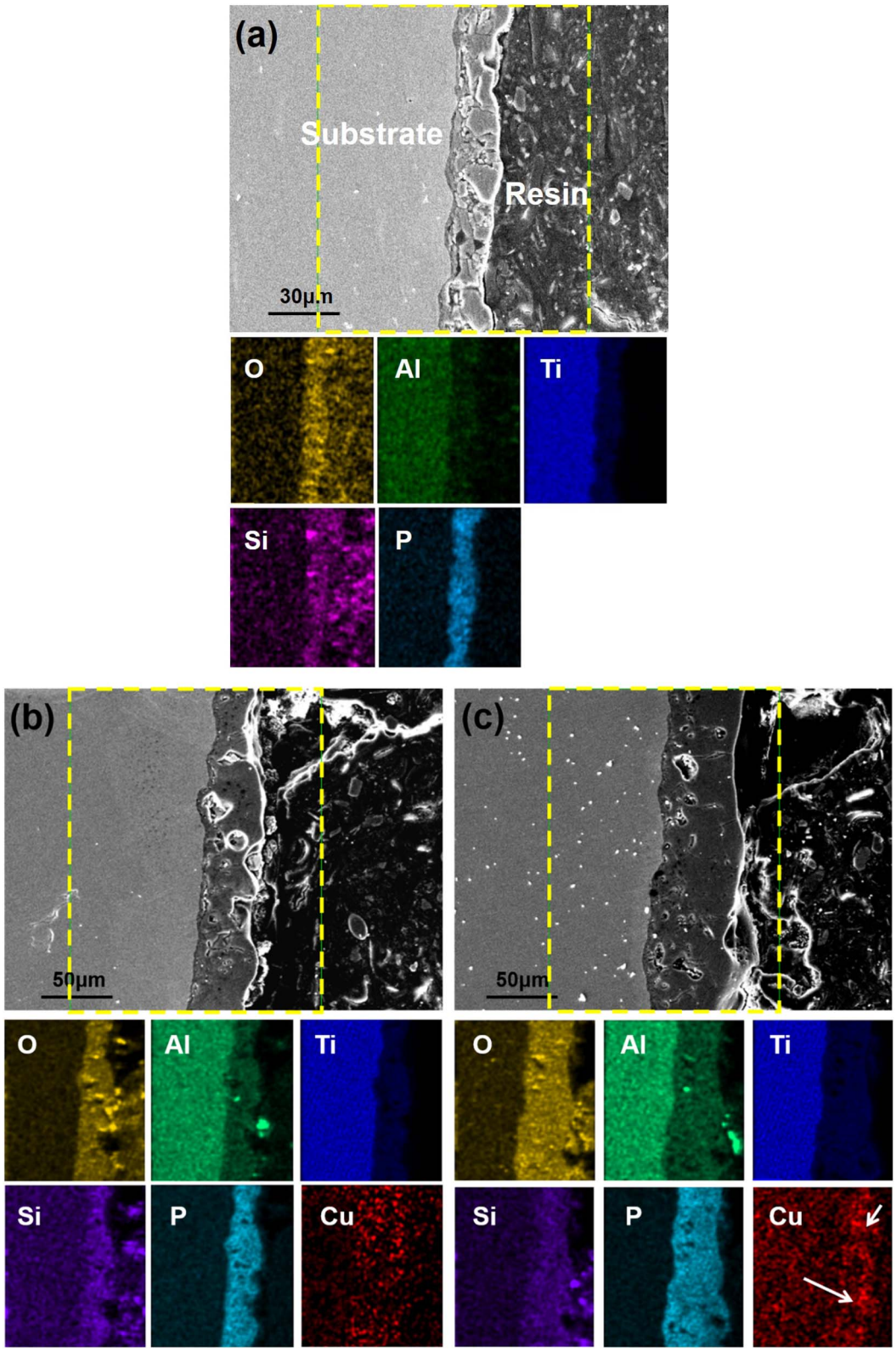

Fig. 4 Cross-section and EDS morphologies of the MAO coating obtained in electrolytes with different contents of Cu nanoparticles, (a) base electrolyte, (b) with 1 g L^{-1} Cu nanoparticles, (c) with 2 g L^{-1} Cu nanoparticles.

demonstrating that Cu in the coating is mainly Cu and CuO. Cu has two characteristic peaks in the $2p_{1/2}$ and $2p_{3/2}$ orbitals with binding energies of 952.2 eV and 932.1 eV.[34,35] In contrast, CuO has two characteristic peaks at 953.4 eV and 933.7 eV,[36,37] while there is a weak satellite peaks of CuO at 943.1 eV with shake-up structure.[38] The corresponding ratio of Cu and Cu^{2+}

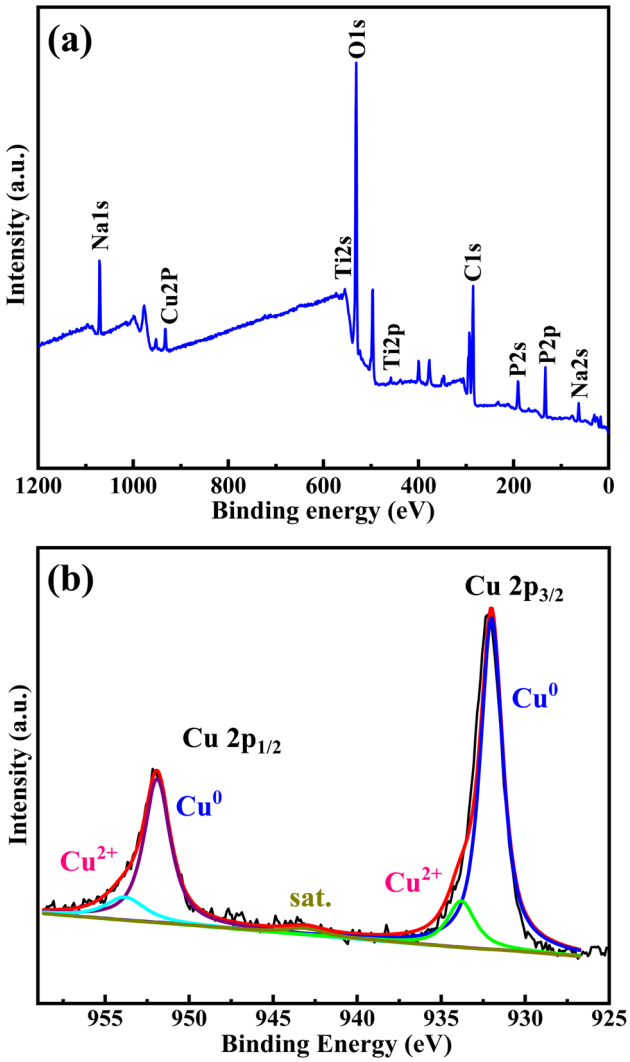

Fig. 5 (a) XPS full spectrum of the MAO coating fabricated in the electrolyte containing 2 g L^{-1} Cu nanoparticles, (b) high resolution spectrum of Cu.

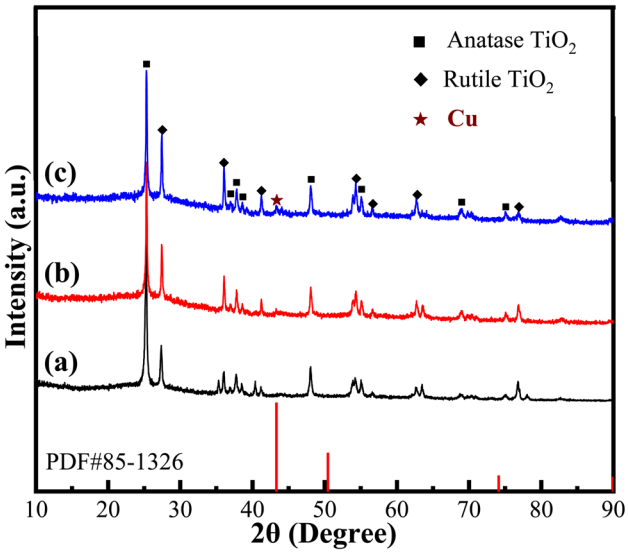

Fig. 6 XRD patterns of the MAO coatings obtained in the electrolytes with different contents of Cu nanoparticles, (a) base electrolyte, (b) with 1 g L^{-1} Cu nanoparticles, (c) with 2 g L^{-1} Cu nanoparticles.

can be quantitatively analyzed based on the relative areas of two Gaussian–Lorentzian peaks in the XPS spectrum.[39] The results show that the MAO coating contains approximately 67% Cu and 33% CuO. The Cu particles react with OH^- in the alkaline electrolyte to form a layer of $Cu(OH)_2$ outside. During the MAO coating formation process, the $Cu(OH)_2$ in the outer layer of the Cu particles is converted to CuO. In addition, some of the Cu particles that enter the coating would be oxidized to CuO during the subsequent MAO process. According to ref. 37 and 40, the MAO coating obtained in the electrolyte containing Cu particles has a dark gray color due to the presence of black CuO.

3.4. Phase structures

Fig. 6 presents the XRD patterns of the MAO coating produced in electrolytes containing varying concentrations of Cu particles. All three oxide coatings comprise anatase TiO_2 and rutile TiO_2. In the spark discharge stage, the oxide melt emitted from the discharge channels forms amorphous TiO_2 under the rapidly cooling effect of the surrounding electrolyte. Amorphous TiO_2 then would convert to anatase TiO_2 under the impact of the subsequent high-temperature discharge spark. With the increasing voltage, the discharge reaction becomes more intense, and part of the internally accumulated anatase TiO_2 transforms into rutile TiO_2 with better thermal stability at a higher temperature.[41] Due to the low content of Cu in the MAO coatings, only one diffraction peak related to Cu (111) appears in the MAO coatings fabricated in the electrolyte with 1 g L^{-1} Cu particles. The relative intensity of the Cu (111) peak increases as the Cu particle content increases to 2 g L^{-1}, which is consistent with EDS test results. This further proved that Cu particles participated in MAO formation and entered the oxide coating. Although Cu reacted with OH^- in the electrolyte, and the Cu entering the oxide coating would be partially oxidized, it still existed mainly in the form of Cu in the MAO coating.

3.5. Coating hardness

Fig. 7 displays the hardness of the MAO coatings. The hardness of the MAO coating obtained in the electrolyte with 0 g L^{-1}, 1 g L^{-1}, and 2 g L^{-1} Cu particles is about 420 HV, 460 HV, and 470 HV, respectively. As is commonly known, the hardness of pure copper is relatively low, typically ranging from 50 to 100 HV.[42,43] The incorporation of soft Cu particles in the MAO coating did not reduce the microhardness of the coating but increased it by about 16.7% and 25.6%, respectively. Because the hardness value of the MAO coating is related to its phase composition, the density of the coating also has an essential effect on the hardness. As shown in Fig. 7, adding Cu particles enhances the densification of the MAO coatings, and the improvement in densification contributes to increasing the hardness of the coatings.

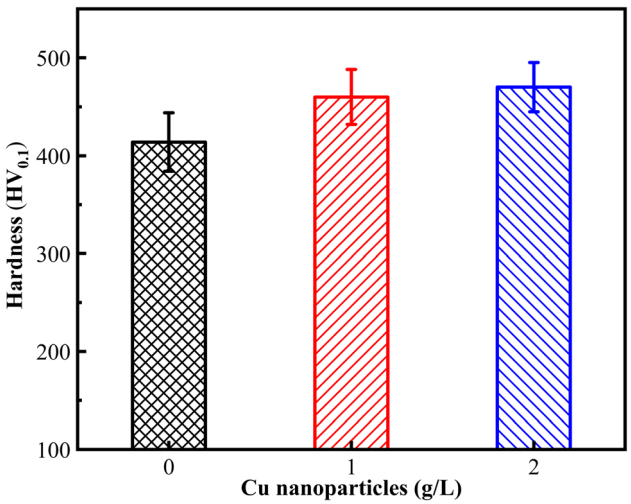

Fig. 7 Hardness of the MAO coating obtained in electrolytes with different contents of Cu nanoparticles.

3.6. Tribological characteristics

After the friction test, it can be seen that the base MAO coating has been thoroughly worn through, and the titanium alloy matrix has leaked out. The MAO coatings' friction coefficient and wear volume are shown in Fig. 8. The friction coefficient of the base MAO coating rapidly increases to approximately 0.93 within the first few seconds of the test, and the higher friction coefficient indicates that the coating surface is coarse. Then, the friction coefficient gradually declines to about 0.45 within 300 s. Afterwards, the friction coefficient fluctuates drastically, ranging from 0.4 to 0.7 within 300–1200 s. After a period of testing, the coating is entirely worn through due to the thin thickness of the base MAO coating, and the stainless steel ball is in contact with the titanium alloy. The temperature of the contact surface between titanium alloy and stainless steel increases during the sliding friction process, and cold welding or gluing of the two occurs in certain micro-areas, which increases the friction force instantaneously, thus causing fluctuations in the coefficient of friction.[44] The friction coefficients of the two MAO coatings containing Cu coatings showed similar trends. The friction coefficient increases rapidly at the beginning of 100–200 s, then rises slowly and stabilizes at about 0.7. Due to the roughness of the MAO coating surface, the beginning stage is the friction between the bulges on the coating surface and the stainless steel ball, which leads to a rapid increase in the friction coefficient. Afterward, the convex parts on the MAO coating are gradually smoothed out under conflict, making the friction coefficient stable. As a result, the friction coefficient of the MAO coating obtained in the electrolyte containing 2 g L^{-1} Cu particles reaches stabilization in a shorter time due to its better densification.

Fig. 8(b) presents the wear volume of the three oxide coatings after the friction test. The wear volume of the base MAO coating is approximately 13.055 × 10^{-2} mm^3. At the same time, the two Cu-containing MAO coatings are 5.985 × 10^{-2} mm^3 and 3.555 × 10^{-2} mm^3, which reduces the wear volume by approximately 54% and 72%, compared with the base coating. It demonstrates that incorporating Cu particles in the MAO coating stabilizes the friction process and significantly reduces the wear volume of the oxide coating. According to the wear volume, the tribological property of the MAO coating obtained in the electrolyte with 2 g L^{-1} Cu particles is about 3.6 times higher than that of the base coating.

Fig. 9 illustrates the friction topography of the three MAO coatings. The central blue area in Fig. 9(a) indicates that the base MAO coating is completely worn through here, exposing the Ti alloy substrate. As indicated by the red arrows, typical plow-like abrasion marks, accompanied by coating flaking, appear in the surrounding area. These phenomena demonstrate that the base MAO coating undergoes severe wear during friction, and tribological mechanisms are primarily abrasive wear and flake-off. The tribological properties of the oxide coating fabricated in the electrolyte containing 1 g L^{-1} Cu particles are greatly improved, with no wear-through, as demonstrated in Fig. 9(b). The coating formed in the electrolyte containing 2 g L^{-1} Cu particles is much slighter, and the friction marks are much shallower, as illustrated in Fig. 9(c). The two MAO coatings incorporating Cu have a dense and stable

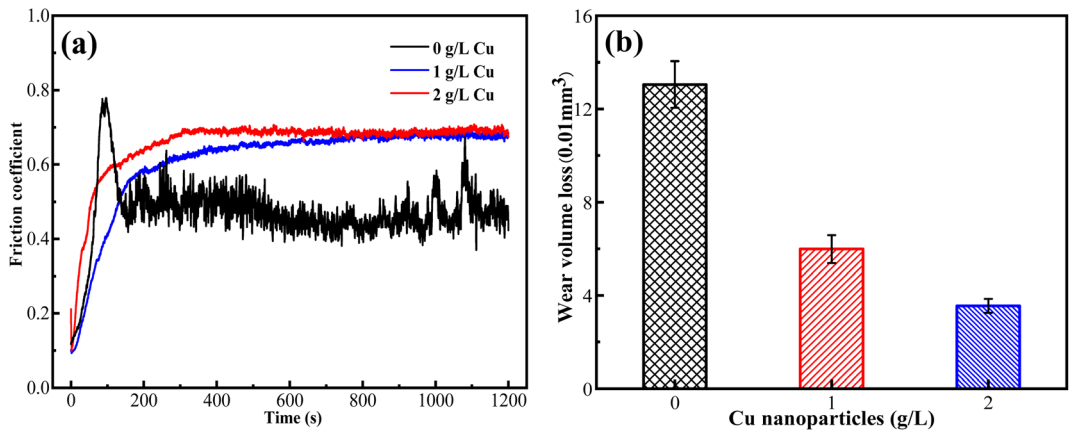

Fig. 8 Friction coefficient curves (a) and wear volume (b) of the MAO coatings obtained in electrolytes with different contents of Cu nanoparticles.

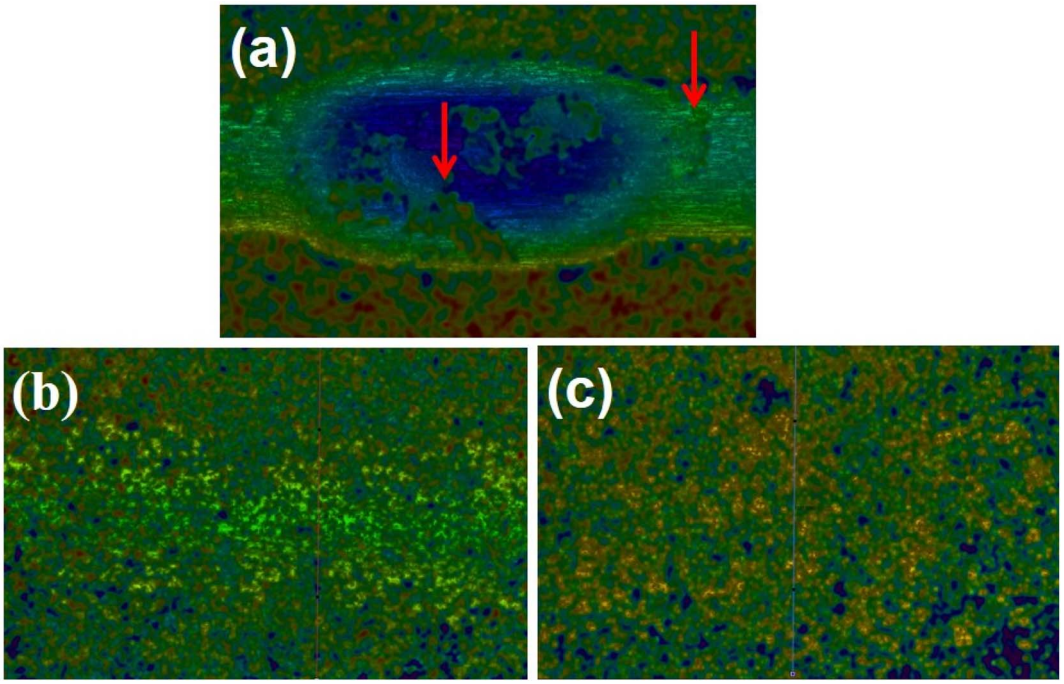

Fig. 9 Friction wear traces of the MAO coatings obtained in electrolytes with different contents of Cu nanoparticles, (a) base electrolyte, (b) with 1 g L^{-1} Cu nanoparticles, (c) with 2 g L^{-1} Cu nanoparticles.

structure, and the form of wear with the stainless steel balls is adhesive wear, corresponding to the friction coefficient and wear volume (Fig. 8(b)).

4. Discussion

The results of various analytical tests indicate that the overall doping of Cu particles in the MAO coating is low, and only about 3 at% in the electrolyte with a content of 2 g L^{-1} Cu particles, which may be due to a combination of several factors. Solid particles in the electrolyte can be driven by the electric field, and particles with sufficient negative charge (due to the adsorption of negative ions) migrate to the anode surface at a higher electrophoretic speed. This is one of the key steps in the process of deposition of particles into the MAO coating. In addition, by stirring the solution, the particles reach the boundary layer of the anode surface under hydrodynamic action. Subsequently, the particles pass through this boundary layer through diffusion and get closer to the titanium alloy surface. When the Cu particles reach the anode surface, they will stay on the anode surface through adsorption. Although the Cu particles in the alkaline electrolyte are negatively charged, the absolute value of the zeta potential is small, making it difficult to enter the discharge channel under the driving force of the electric field. Therefore, Cu particles are mainly deposited in the oxide coating by adhering to the discharge melt on the anode surface under mechanical agitation, which leads to a small number of Cu particles entering the MAO coating.[7,45] Finally, Cu particles have good electrical conductivity, and excessive doping in the oxide coating is bound to reduce the insulating property of the coating, increase the intensity of spark discharge, cause electrical ablation, and even lead to the oxide film spalling off. Consequently, the MAO coating formed from the electrolyte containing 3 g L^{-1} Cu particles is thin and has a non-uniform surface.

After the start of MAO, anodic oxidation reactions occur on the titanium alloy surface, forming an oxide coating mainly composed of anatase TiO_2, accompanied by O^{2-} being oxidized to generate O_2 escaping. At this stage, limited by the particle size and low zeta potential value of the Cu particles, only a few Cu particles can be deposited on the anode surface. When the voltage reaches a certain critical value, discharge channels form on the anode surface, creating a high temperature and high-pressure environment in the channels. These channels provide paths for the deposition of Cu particles. As a result of transient high temperatures, micro-zone melting occurs on the substrate surface, leading to physical and chemical reactions with the electrolyte entering the discharge channel. Whereafter, the molten product is discharged from the discharge channel and solidifies on the anode surface to form an oxide coating containing electrolyte components as the electrolyte rapidly cools, which is the reason that the MAO coating appears to have pores and cracks on the surface, like craters. Under mechanical stirring, some Cu particles adhere to the melt produced by the microarc discharges and are deposited in the MAO coating, as illustrated in Fig. 10(b). Consequently, the Cu element is mainly distributed outside of the MAO coating. Thus, microzone discharge and mechanical agitation are critical in incorporating Cu particles into the MAO coatings, which is consistent with M. Shokouhfar's study of factors affecting nanoparticle incorporation.[46]

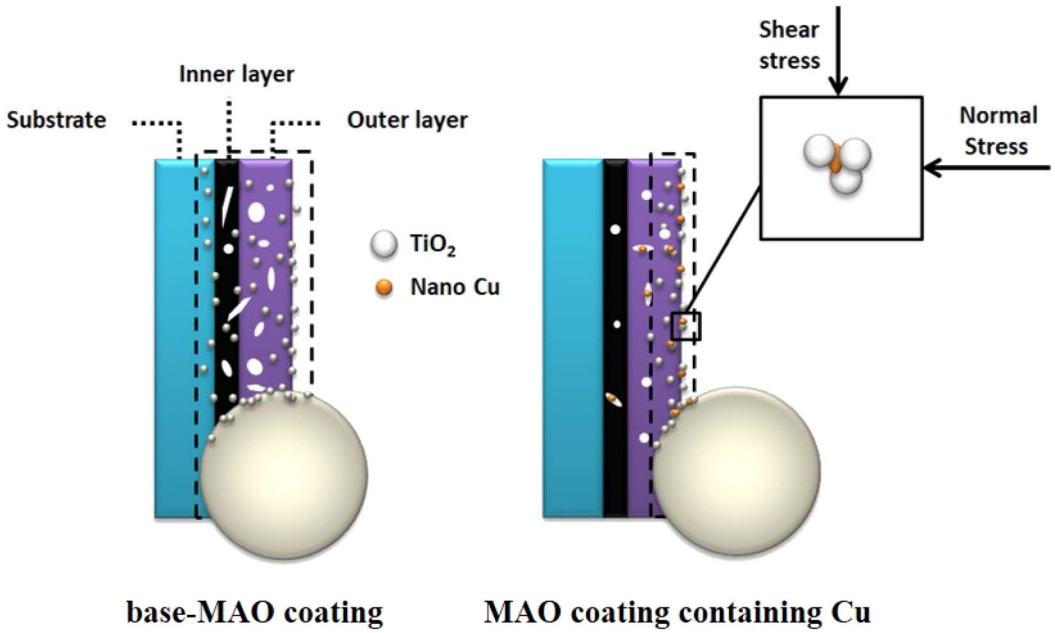

Fig. 10 Diagram of the grinding reduction mechanism of Cu nanoparticles.

Incorporating Cu particles improves the friction properties of the MAO coatings with more stable friction coefficients and less wear volume than the base MAO coating. This is because adding Cu creates composite MAO coatings with density structures. As shown in Fig. 4, adding Cu particles to the electrolyte enhanced the density of the outer layer of the MAO coating. In the early stage of the microarc discharge, the discharge sparks are tiny and uniform. The anode surface of the melt accumulation is uniform, and incorporated Cu particles can significantly decrease the number and size of pores, making the MAO coating dense. In the middle and late stages of MAO, Cu particles play the role of mechanical stirring to break the bubbles generated on the MAO coating. The air bubbles become smaller, accelerate the escape, and play a role in reducing the external loose layer of the MAO coating. The deposition of Cu particles is helpful to fill the micropores and cracks in the MAO coating, and improve the density and overall performance of the coating. In addition, the Cu-containing composite MAO coatings are composed of anatase TiO_2, rutile TiO_2, and a small amount of Cu. The hardness of nano Cu is about 80–100 HV, and the hardness of TiO_2 can reach over 1000 HV.[47,48] The MAO coating's Cu and TiO_2 (anatase and rutile) form a soft–hard composite structure. The excellent plasticity of the Cu in the composite coating is crucial for enhancing the friction properties of the coating. However, the results show that the MAO coating containing Cu has a higher coefficient of friction than the base coating, while the wear volume is lower. Fig. 10 displays a simplified diagram of the tribological mechanisms of the MAO coatings. Due to the presence of many bumps and holes on the surface of the MAO coating, when the brittle area outside the MAO coating is destroyed after the sliding friction begins, the formed abrasive particles adhere to the surface of the MAO coating and the stainless steel ball. For the soft and hard composite MAO coating containing Cu, the Cu particles in the grinding chips have plastic deformation, and some Cu is gradually transferred and adhered to the stainless steel ball. Eventually, a copper layer slowly forms on the contact surface between the stainless steel ball and the MAO coating, and the friction between the stainless steel and the MAO coating is transformed into friction between Cu and Cu. The coefficient of friction between Cu/Cu ranges from 0.7 to 1.0,[49] which is consistent with the test results. The Cu layer between the friction sub-interfaces plays a role in stabilizing the friction coefficient and reducing the amount of wear. Although the Cu content in the composite MAO coating is small, it can significantly reduce the wear volume of the MAO coating.

5. Conclusion

Grey MAO coatings of anatase type TiO_2 and rutile type TiO_2 were prepared on Ti_6Al_4V titanium alloy in a phosphate-borate electrolyte. Different amounts of Cu particles were added to the base electrolyte, and the results showed that adding Cu particles increased the proportion of rutile TiO_2 in the MAO coating, and Cu and CuO were detected in the coating. In addition, with the increase of Cu particle content in the electrolyte, the MAO coating's thickness, uniformity, density, and color were enhanced. However, the thickness of the MAO coating decreased, and the spalling occurred due to the excessive concentration of Cu particles. In the electrolyte with 2 g L^{-1} Cu particle, the MAO coating thickness increased by approximately 109% compared to the base coating. It is worth noting that mechanical agitation facilitated the adsorption of suspended Cu particles onto molten oxide produced by spark discharge; consequently, most Cu was found outside rather than within the oxide coating. Adding Cu particles to the electrolyte formed a composite MAO coating with a soft and hard combination on the titanium alloy's surface. Compared with the

base MAO coating, the composite coating had a stable friction coefficient and small wear volume.

Data availability

The authors confirm that the data supporting the findings of this study are available within the article.

Conflicts of interest

There are no conflicts to declare.

Acknowledgements

This work was supported by the Henan Provincial Science and Technology Research Project (Grant No. 242102221040, 242102220010); and the Special Funding and Equipment Support of the Visiting Professor at the School of Materials Science and Engineering (4001-40734).

References

1 F. Yin, S. Ma, S. Hu, Y. Liu, L. Hua and G. J. Cheng, Understanding the microstructure evolution and mechanical behavior of titanium alloy during electrically assisted plastic deformation process, *Mater. Sci. Eng. A*, 2023, **869**, 144815.

2 Z. Wu, H. Kou, N. Chen, Z. Xi, J. Fan, B. Tang and J. Li, Recent developments in cold dwell fatigue of titanium alloys for aero-engine applications: a review, *J. Mater. Res. Technol.*, 2022, **20**, 469–484.

3 X. Han, J. Ma, A. Tian, Y. Wang, Y. Li, B. Dong, X. Tong and X. Ma, Surface modification techniques of titanium and titanium alloys for biomedical orthopaedics applications: a review, *Colloid. Surface. B*, 2023, **227**, 113339.

4 G. Li, F. Ma, P. Liu, S. Qi, W. Li, K. Zhang and X. Chen, Review of micro-arc oxidation of titanium alloys: mechanism, properties and applications, *J. Alloys Compd.*, 2023, **948**, 169773.

5 M. Molaei, A. Fattah-Alhosseini and M. K. Keshavarz, Influence of different sodium-based additives on corrosion resistance of PEO coatings on pure Ti, *J. Asian Ceram. Soc.*, 2019, **7**(2), 247–255.

6 F. Xi, X. Zhang, X. Jiang, Y. Kang, X. Wen and Y. Liu, Growth mechanism of oxide layer on Ti-6Al-4V substrate with different surface topographies during the early stage of micro-arc oxidation, *Surf. Coat. Technol.*, 2023, **467**, 129685.

7 M. Kaseem, S. Fatimah, N. Nashrah and Y. G. Ko, Recent progress in surface modification of metals coated by plasma electrolytic oxidation: principle, structure, and performance, *Prog. Mater. Sci.*, 2021, **117**, 100735.

8 H. Chen, Y. Ren, D. Jian, Y. Chen and J. Hao, Research Progress of Micro-arc Oxidation Antibacterial Film Doped with Particles, *Rare Met. Mater. Eng.*, 2023, **52**, 745–752.

9 A. Fattah-alhosseini, M. Molaei, N. Attarzadeh, K. Babaei and F. Attarzadeh, On the enhanced antibacterial activity of plasma electrolytic oxidation (PEO) coatings that incorporate particles: a review, *Ceram. Int.*, 2020, **46**, 20587–20607.

10 X. Lu, M. Mohedano, C. Blawert, E. Matykina, R. Arrabal, K. U. Kainer and M. L. Zheludkevich, Plasma electrolytic oxidation coatings with particle additions – a review, *Surf. Coat. Technol.*, 2016, **307**, 1165–1182.

11 A. Fattah-alhosseini, R. Chaharmahali and K. Babaei, Effect of particles addition to solution of plasma electrolytic oxidation (PEO) on the properties of PEO coatings formed on magnesium and its alloys: a review, *J. Magnes. Alloy*, 2020, **8**, 799–818.

12 E. Nikoomanzari, A. Fattah-alhosseini, M. Karbasi and A. Nourian, A versatile TiO_2/ZrO_2 nanocomposite coating produced on Ti-6Al-4V via plasma electrolytic oxidation process, *Surf. Interfaces*, 2022, **32**, 102128.

13 W. Wang, C. Xin, Z. Feng, G. Li, R. Zhang, J. Hu, M. Tang, Y. Liu and W. Zhang, Ceramic coatings by microarc oxidation of Ti and Al alloys, *Surf. Interfaces*, 2022, **33**, 102260.

14 X. Li, C. Dong, Q. Zhao, Y. Pang, F. Cheng and S. Wang, Characterization of Microstructure and Wear Resistance of PEO Coatings Containing Various Microparticles on Ti6Al4V Alloy, *J. Mater. Eng. Perform.*, 2018, **27**, 1642–1653.

15 S. M. Li, W. H. Yao, J. H. Liu, M. Yu and K. Ma, Effect of SiC nanoparticle concentration on the properties of oxide films formed on Ti-10V-2Fe-3Al alloy, *Vacuum*, 2016, **123**, 1–7.

16 M. Mu, X. Zhou, Q. Xiao, J. Liang and X. Huo, Preparation and tribological properties of self-lubricating TiO_2/graphite composite coating on Ti6Al4V alloy, *Appl. Surf. Sci.*, 2012, **258**, 8570–8576.

17 M. Mu, J. Liang, X. Zhou and Q. Xiao, One-step preparation of TiO_2/MoS_2 composite coating on Ti6Al4V alloy by plasma electrolytic oxidation and its tribological properties, *Surf. Coat. Technol.*, 2013, **214**, 124–130.

18 Y. Tuo, Z. Yang, Z. Guo, Y. Chen, J. Hao, Q. Zhao, Y. Kang, Y. Zhang and Y. Zhao, Pore structure optimization of MoS_2/Al_2O_3 self-lubricating ceramic coating for improving corrosion resistance, *Vacuum*, 2023, **207**, 111687.

19 J. Cheng, M. Mao, X. Gan, Q. Lei, Z. Li and K. Zhou, Microstructures, mechanical properties, and grease-lubricated sliding wear behavior of Cu-15Ni-8Sn-0.8Nb alloy with high strength and toughness, *Friction*, 2021, **9**, 1061–1076.

20 V. Hutsaylyuk, M. Student, V. Posuvailo, O. Student, Y. Sirak, V. Hvozdets'kyi, P. Maruschak and H. Veselivska, The properties of oxide-ceramic layers with Cu and Ni inclusions synthesizing by PEO method on top of the gas-spraying coatings on aluminium alloys, *Vacuum*, 2020, **179**, 109514.

21 D. Zhao, J. Guo and X. Li, Structure and Wear Behavior of Cu/Graphite Composite Coating Electroplated on TC4 Alloy, *Rare Met. Mater. Eng.*, 2020, **49**, 2861–2868.

22 J. Li, H. Zhang, A. Fan and B. Tang, Tribological properties characterization of Ti/Cu/N thin films prepared by DC magnetron sputtering on titanium alloy, *Surf. Coat. Technol.*, 2016, **294**, 30–35.

23 Y. Yang, S. Cao, S. Zhang, C. Xu and G. Qi, Microstructure and wear resistance of Ti–Cu–N composite coating prepared via laser cladding/laser nitriding technology on Ti–6Al–4V alloy, *Appl. Phys. A*, 2017, **123**, 474.

24 M. Zhang, L. Zhu, J. Wang, N. Ye, S. Dai, S. Yu and Y. Wu, Surface modification of biomedical metals by double glow plasma surface alloying technology: a review of recent advances, *J. Mater. Res. Technol.*, 2023, **24**, 3423–3452.

25 H. Tan, Y. Guo, D. Wang and Y. Cui, The development of a Cu@Graphite solid lubricant with excellent anti-friction and wear resistant performances in dry condition, *Wear*, 2022, 488–489.

26 G. Greczynski and L. Hultman, C 1s peak of adventitious carbon aligns to the vacuum level: dire consequences for material's bonding assignment by photoelectron spectroscopy, *ChemPhysChem*, 2017, **18**, 1507–1512.

27 G. Greczynski and L. Hultman, Reliable determination of chemical state in x-ray photoelectron spectroscopy based on sample-work-function referencing to adventitious carbon: resolving the myth of apparent constant binding energy of the C 1s peak, *Appl. Surf. Sci.*, 2018, **451**, 99–103.

28 G. Greczynski and L. Hultman, X-ray photoelectron spectroscopy: towards reliable binding energy referencing, *Prog. Mater. Sci.*, 2020, **107**, 100591.

29 G. Greczynski and L. Hultman, Compromising science by ignorant instrument calibration—need to revisit half a century of published XPS data, *Angew. Chem., Int. Ed.*, 2020, **59**, 5002–5006.

30 G. Greczynski and L. Hultman, The same chemical state of carbon gives rise to two peaks in X-ray photoelectron spectroscopy, *Sci. Rep.*, 2021, **11**, 1–5.

31 J. A. Phys and L. Hultman, A step-by-step guide to perform x-ray photoelectron spectroscopy, *J. Appl. Phys.*, 2022, **132**, 011101.

32 G. Greczynski, R. T. Haasch, N. Hellgren, E. Lewin and L. Hultman, X-ray photoelectron spectroscopy of thin films, *Nat. Rev. Methods Primers*, 2023, **3**, 40.

33 P. Zhang a, F. Chu, M. Zhou, B. Tao and F. Miao, DSSC using natural dye sensitized and Ag/CdS/TiO_2 composite structured light anode, *Vacuum*, 2024, **219**, 112763.

34 N. Karikalan, R. Karthik, S. Chen, C. Karuppiah and A. Elangovan, Sonochemical Synthesis of Sulfur Doped Reduced Graphene Oxide Supported CuS Nanoparticles for the Non-Enzymatic Glucose Sensor Applications, *Sci. Rep.*, 2017, **7**, 2494.

35 M. Kumar, V. Bhatt, O. S. Nayal, S. Sharma, V. Kumar, M. S. Thakur, N. Kumar, R. Bal, B. Singh and U. Sharma, CuI nanoparticles as recyclable heterogeneous catalysts for C–N bond formation reactions, *Catal. Sci. Technol.*, 2017, **7**, 2857–2864.

36 V. Sudha, G. Murugadoss and R. Thangamuthu, Structural and morphological tuning of Cu-based metal oxide nanoparticles by a facile chemical method and highly electrochemical sensing of sulphite, *Sci. Rep.*, 2021, **11**, 3413.

37 D. Jeong, W. Jo, J. Jeong, T. Kim, S. Han, M. Son and H. Jung, Characterization of Cu_2O/CuO heterostructure photocathode by tailoring CuO thickness for photoelectrochemical water splitting, *RSC Adv.*, 2022, **12**, 2632.

38 J. Wang, Q. Deng, M. Li, K. Jiang, J. Zhang, Z. Hu and J. Chu, Copper ferrites@reduced graphene oxide anode materials for advanced lithium storage applications, *Sci. Rep.*, 2017, **7**, 8903.

39 G. D. Khattak, A. Mekki and M. A. Gondal, Effect of laser irradiation on the structure and valence states of copper in Cu-phosphate glass by XPS studies, *Appl. Surf. Sci.*, 2010, **256**, 3630–3635.

40 Q. Guo, D. Xu, W. Yang, Y. Guo, Z. Yang, J. Li and P. Gao, Synthesis, corrosion, and wear resistance of a black microarc oxidation coating on pure titanium, *Surf. Coat. Technol.*, 2020, **386**, 125454.

41 S. Vargas-Villanueva, J. P. Velásquez-Tamayo, D. A. Torres-Cerón, D. F. Mercado, R. A. Torres-Palma, D. Riassetto, J. S. Riva, S. Amaya-Roncancio, S. F. Castilla-Acevedo and E. Restrepo-Parra, Impact of the duty cycle on the morphology and photocatalytic properties of S-TiO_2 obtained by plasma electrolytic oxidation to treat real electroplating wastewater contaminated with Cr^{6+}, *J. Environ. Chem. Eng.*, 2023, **11**, 110246.

42 K. Singh, V. Khanna, S. Singh, S. A. Bansal, V. Chaudhary and A. Khosla, Paradigm of state-of-the-art CNT reinforced copper metal matrix composites: processing, characterizations, and applications, *J. Mater. Res. Technol.*, 2023, **24**, 8572–8605.

43 A. Jamwal, P. Mittal, R. Agrawal, S. Gupta, D. Kumar, K. K. Sadasivuni and P. Gupta, Towards sustainable copper matrix composites: manufacturing routes with structural, mechanical, electrical and corrosion behaviour, *J. Compos. Mater.*, 2020, **54**, 2635–2649.

44 Y. M. Wang, B. L. Jiang, L. X. Guo and T. Q. Lei, Antifriction property of microarc oxidation coating on titanium alloy under solid lubricating sliding condition, *Surf. Rev. Lett.*, 2004, **11**, 367–372.

45 M. O'Hara, S. C. Troughton, R. Francis and T. W. Clyne, The incorporation of particles suspended in the electrolyte into plasma electrolytic oxidation coatings on Ti and Al substrates, *Surf. Coat. Technol.*, 2020, **385**, 125354.

46 M. Shokouhfar and S. R. Allahkaram, Formation mechanism and surface characterization of ceramic composite coatings on pure titanium prepared by micro-arc oxidation in electrolytes containing nanoparticles, *Surf. Coat. Technol.*, 2016, **291**, 396–405.

47 A. A. Volinsky, J. Vella, I. S. Adhihetty, V. Sarihan, L. Mercado, B. H. Yeung and W. W. Gerberich, Microstructure and mechanical properties of electroplated Cu thin films, *MRS Online Proc. Libr.*, 2000, **649**, 53.

48 Y. Zhou, X. Wu, G. Xu, B. Li, H. Zhang, L. Du and Z. Li, Synthesis, microdefect and mechanical properties of large bulk nanocrystalline silver and copper, *Chin. J. Nonferrous Metals*, 2000, **10**, 455–459.

49 C. Wang, J. Liu, T. Wei and H. Chen, *Tribological Materials and Surface Engineering*, National Defense Industry Press, Beijing, 2012, p. 36.